The appearance of boundary layers and drift flows due to high-frequency surface waves

Ofer Manor, Leslie Y. Yeo and James R. Friend

Link to this article: http://journals.cambridge.org/abstract_S0022112012002935

How to cite this article:
Ofer Manor, Leslie Y. Yeo and James R. Friend (2012). The appearance of boundary layers and drift flows due to high-frequency surface waves. Journal of Fluid Mechanics,707, pp 482-495
doi:10.1017/jfm.2012.293

Request Permissions : Click here

The appearance of boundary layers and drift flows due to high-frequency surface waves

Ofer Manor[1,2], **Leslie Y. Yeo**[1] **and James R. Friend**[1,2]†

[1] MicroNanophysics Research Laboratory, School of Electrical and Computer Engineering, RMIT University, Melbourne, VIC 3001, Australia

[2] The Melbourne Centre for Nanofabrication, Clayton, VIC 3800, Australia

The classical Schlichting boundary layer theory is extended to account for the excitation of generalized surface waves in the frequency and velocity amplitude range commonly used in microfluidic applications, including Rayleigh and Sezawa surface waves and Lamb, flexural and surface-skimming bulk waves. These waves possess longitudinal and transverse displacements of similar magnitude along the boundary, often spatiotemporally out of phase, giving rise to a periodic flow shown to consist of a superposition of classical Schlichting streaming and uniaxial flow that have no net influence on the flow over a long period of time. Correcting the velocity field for weak but significant inertial effects results in a non-vanishing steady component, a drift flow, itself sensitive to both the amplitude and phase (prograde or retrograde) of the surface acoustic wave propagating along the boundary. We validate the proposed theory with experimental observations of colloidal pattern assembly in microchannels filled with dilute particle suspensions to show the complexity of the boundary layer, and suggest an asymptotic slip boundary condition for bulk flow in microfluidic applications that are actuated by surface waves.

1. Introduction

The interaction between acoustic waves and boundary layer flow has been investigated since the 18th century, when Chladni (1787) demonstrated the organization of small particles of different size into distinct patterns associated with nodes, the regions devoid of transverse vibration, in a vibrating metal plate; Faraday (1831) later found the particle displacement and counterintuitive alignment at antinodal points is due to air currents induced by acoustic streaming. Acoustic streaming was further studied in the context of Kundt's tubes and particle collection from the mid-1800s to the early 20th century (Hutchisson & Morgan 1931); Rayleigh (1884) and Schlichting (1932) showed a stationary (or standing) acoustic wave at or near a solid boundary induces fluid motion within an adjacent boundary layer, commonly referred to as Schlichting streaming or as the Schlichting boundary layer. The layer is equivalent to the Stokes boundary layer when the acoustic wavelength is much larger than the boundary layer thickness, and is governed by viscous dissipation and weak

† Email address for correspondence: james.friend@rmit.edu.au

inertia that lead to periodic vortices and a steady drift velocity at the outer edge of the boundary layer.

Early studies examined the influence of low-frequency stationary acoustic waves on the Schlichting boundary layer. Rayleigh (1884) investigated flow patterns in Kundt's tubes and showed that the boundary layer comprises four separate vortical cells per wavelength along the solid substrate, generating a steady drift velocity at the outer edge of the boundary layer. Schlichting (1932) subsequently extended this work to predict the flow above a solid vibrating substrate with either transverse or longitudinal stationary surface waves of the form $u_S(x, t) = A(x) \cos \omega t$, where u_S is the velocity at the solid boundary and A, ω, x and t are the velocity amplitude, angular frequency, spatial coordinate along the solid boundary, and time, respectively. He found the drift velocity takes the form

$$u_d = -(3A/4\omega)\partial_x A. \tag{1.1}$$

This result was extended and verified for flow fields around tangentially or radially oscillating cylinders (Holtsmark *et al.* 1954; Riley 1965, 1986; Secomb 1978; Wang 2005). In other work, Longuet-Higgins (1953) conducted a comprehensive study on the influence of shallow waves on the flow field in and out of the boundary layer; this was extended by Nyborg (1952), Stuart (1966), Riley (1998, 2001) and Westervelt (2004) to include excitation of the boundary layer by general periodic flows in the bulk of a fluid far from the solid boundary (bulk waves). Stuart (1966) further suggested that the Schlichting boundary layer flow may generate high-Reynolds-number flow in its vicinity, giving rise to a second, external boundary layer. The boundary layer flow was found to satisfy (1.1) throughout, whether the excitation is along or transverse to the solid boundary (but not both), and whether the source of excitation is from the fluid bulk or the solid boundary. These assumptions and (1.1), however, are not satisfied under the excitation of two-dimensional boundary surface waves (SWs), encompassing Rayleigh and Sezawa surface acoustic waves (the symmetric and antisymmetric modes of a surface acoustic wave or SAW) and bulk acoustic waves including Lamb, surface-skimming bulk acoustic waves (SSBWs) and flexural waves. At the solid surface, these waves possess displacement components both along and transverse to the surface, contributing to the formation of a boundary layer and a drift velocity not properly predicted by past analyses, especially when generated at ultrasonic frequencies in modern actuation of microfluidic systems using high-frequency piezoelectric actuators.

Fluid phenomena induced by such two-dimensional and high-frequency SWs are being used for microfluidics in a diverse set of novel ways: to generate flow in microchannels (Girardo *et al.* 2008; Tan, Yeo & Friend 2009), concentrate and separate particles (Dorrestijn *et al.* 2007; Li, Friend & Yeo 2008; Shi *et al.* 2009), mix liquids (Luong, Phan & Nguyen 2011), displace drops (Hodgson *et al.* 2009; Brunet *et al.* 2010), atomize liquids (Qi, Yeo & Friend 2008) and pattern particle aggregates (Alvarez, Friend & Yeo 2008; Zeng *et al.* 2010). Applications of this burgeoning technology are mainly in the fields of medicine and biology in the form of microscale laboratories for drug screening, drug delivery and point-of-care diagnostics among others (Wixforth *et al.* 2004; Yeo & Friend 2009; Friend & Yeo 2011; Nam *et al.* 2011). There are several flow types that may appear simultaneously under the excitation of SWs (Lighthill 1978), the most significant of which are Eckart streaming (Eckart 1948) and Schlichting boundary layer flow. Eckart streaming is understood, at least under weak excitation, to emerge from the viscous attenuation of sound waves in a fluid, generating vortical steady flow patterns in the bulk of the fluid.

However, neither the structure of the Schlichting boundary layer nor its effects on flow in microfluidics is understood due to the absence of theory that properly treats the two-dimensional aspect of surface waves. A model generalized to allow non-stationary acoustic wave propagation along the solid–fluid interface is necessary, and such a model is derived and provided below.

We find substantial discrepancies in Schlichting boundary layer flow from predictions based on classical theory with excitation of two-dimensional SWs at megahertz-order frequencies ($\omega/2\pi \sim 10^6$–10^8 Hz). Owing to the periodicity of these mostly harmonic flow fields, their direct influence on the flow vanishes over long time scales ($t \gg 2\pi/\omega \sim 10^{-6}$–$10^{-8}$ s), a well-known result. However, the leading-order periodic flow field only sets the stage for what arises via higher-order interactions: the drift flow, the steady component of the inertial secondary flow field. Furthermore, we find the drift velocity in the fluid bulk, appearing as a consequence of the two-dimensional, spatiotemporally varying SW that form a very thin boundary layer, typically less than 1 µm thick. The drift velocity is larger in magnitude than the classic result that appears from one-dimensional acoustic waves that satisfy (1.1). Finally, the relationship between the form of the induced SW and the drift flow is more complex than what is shown in the classical theory. With the classical approach embodied by the result in (1.1), a spatial gradient in the wave vibration velocity A is necessary to induce a drift flow, and reversal of the phase of the SW from prograde to retrograde exhibits no change in the drift flow behaviour. Including the two-dimensional aspect of the SW allows the generation of a drift flow even from a SW that has no spatial amplitude variation, and also properly exhibits a reversal in drift flow when the phase of the SW is reversed.

Using both theory and experiment we show that secondary bulk waves appear in a microchannel due to SW transmission into the fluid bulk and reflection from the fluid–channel wall interface. These secondary bulk waves are shown to influence the flow field within the Schlichting boundary layer concurrently with the SWs, and thus give rise to a complex flow field that conserves properties of both the bulk waves and SWs. The generation of these secondary bulk waves has tremendous importance in microfluidic systems typically composed of closed structures and free fluid surfaces, all excellent reflectors of acoustic waves. These details are confirmed via patterning of microparticles suspended in water in a carefully designed experiment.

In §2 we derive the drift velocity in a half space under the excitation of a generalized two-dimensional SWs and under the mutual excitation of a SW and a corresponding stationary bulk wave that we expect to appear between two gas/liquid stress-free boundaries, such as in our experimental system. We then compare the results of our theory with a model experiment in §3 to confirm the validity of the theoretical analysis. Finally, we conclude by summarizing our findings in §4.

2. Theory

Consider the half space of a fluid above a solid substrate illustrated in figure 1(*a*); the coordinates x and y are measured along and transverse to the fluid–solid boundary $y = 0$. A harmonic SW propagating on the boundary $y = 0$ with increasing x is composed of longitudinal and transverse displacements of similar amplitude, the velocities of which are given by the form

$$(u_x, u_y)_{y=0} = (\chi U \exp(\mathrm{i}(\omega t - kx) - \alpha x), U \exp(\mathrm{i}(\omega t - kx + \varphi) - \alpha x)), \qquad (2.1)$$
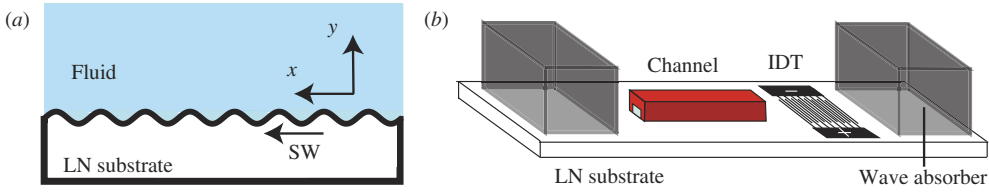
FIGURE 1. (Colour online) (*a*) A wave propagates as (for example) a Rayleigh SW on a lithium niobate (LN) substrate, producing motion along the fluid–solid boundary. (*b*) A microchannel, open on both ends, and placed above the substrate is used as the experimental analogue of (*a*). The SAW is generated by the interdigital transducer (IDT) and is absorbed at both ends of the substrate to avoid reflection and consequent interference.

incorporating propagating wave motion in contrast to the classical treatment where a standing SW was presumed. Here χU and U are the initial velocity magnitudes of the SW longitudinal and transverse components with phase difference φ; k is the wavenumber and α is the SW attenuation coefficient as it propagates in the solid. The real part of (2.1) is the physical SW.

2.1. *Non-dimensionalization*

Following Rosenhead (1963), Stuart (1966), Lighthill (1978) and Riley (1998, 2001), we may ignore compressibility effects in the Schlichting boundary layer by requiring the Mach numbers in the solid $\varepsilon \equiv U/c$ and in the liquid U/c_l and the ratio of the thickness of the boundary layer to the acoustic wavelength in the fluid $\omega/\beta c_l$ to be small. Here, c_l, ρ_l, μ_l are the speed of sound, density and viscosity in the fluid, respectively, and $\beta^{-1} \equiv \sqrt{2\mu/\rho\omega}$ is the characteristic thickness of the boundary layer. Both ε and U/c_l are usually of similar order of magnitude ($\sim 10^{-4}$–10^{-5} in the experiment) since the acoustic phase velocity in both mediums is of a similar order of magnitude.

Utilizing the following transformations, the problem becomes dimensionless:

$$\left.\begin{array}{l} t \to t/\omega, \quad x \to k^{-1}x, \quad y \to \beta^{-1}y, \quad u_x \to Uu_x, \\ u_y \to \eta Uu_y, \quad \alpha \to k\alpha, \quad \psi \to \beta^{-1}U\psi, \end{array}\right\} \tag{2.2}$$

where $\eta \equiv k/\beta \ll 1$ is the ratio between the boundary layer thickness and the SW wavelength and is related to the reciprocal of the Strouhal number; ψ is the streamfunction that satisfies $(u_x, u_y) = (\partial_y\psi, -\partial_x\psi)$. The velocity of the propagating SW in the fluid in (2.1), in dimensionless form, then reads

$$(u_x, u_y)_{y=0} = (\chi \exp^{\mathrm{i}(t-x)-\alpha x}, \eta^{-1} \exp(\mathrm{i}(t - x + \varphi) - \alpha x)). \tag{2.3}$$

Mass and momentum conservation, on the other hand, require (Riley 1998, 2001)

$$\tfrac{1}{2}\partial_y^4\psi = \partial_t(\partial_y^2\psi) + \varepsilon[\partial_y\psi\partial_x(\partial_y^2\psi) - \partial_x\psi\partial_y(\partial_y^2\psi)] + O(\eta^2). \tag{2.4}$$

Two small parameters, $\eta \ll 1$ and $\varepsilon \equiv U/c \ll 1$, appear in (2.3) and (2.4), where $c = \omega/k$ is the SW phase velocity; it is reasonable to require $\varepsilon \ll \varepsilon/\eta \ll 1 \ll 1/\eta$ given the high frequencies $\omega/2\pi \sim O(10^6$–10^8 Hz$)$ and velocity amplitudes $U \sim O(0.01$–1 m s$^{-1})$ typical in SW-actuated microfluidics, shown for ambient water in figure 2. Yeo & Friend (2009) and Friend & Yeo (2011), and references therein provide many examples alongside the experimental study to follow (figure 1*b*).
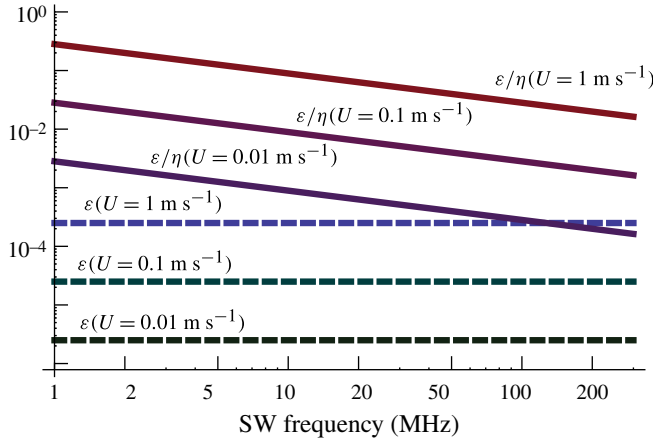
FIGURE 2. (Colour online) Variations in the non-dimensional parameters ε and ε/η over a range of frequencies (1–300 MHz) relevant to microfluidics for water atop 127.68° y-axis rotated, x-axis propagating LN ($c \sim 4000$ m s^{-1}), a typical cut for microfluidics, subject to the Rayleigh SW velocity amplitudes $U = 0.01, 0.1$ and 1 m s^{-1}.

2.2. *Asymptotic expansion*

Since (2.4) represents a boundary layer, an asymptotic flow field, it cannot simultaneously satisfy both the conditions at the solid boundary (2.3) and the decay of the velocity field far from the solid. We then define the velocity at the solid boundary by (2.3) and require u_x to be bounded far from the solid boundary (Stuart 1966). To simplify the mathematical problem (2.3) and (2.4) are expanded in the asymptotic series

$$u_x = \sum_{n=-1}^{\infty} f_n u_{x,n}, \quad u_y = \sum_{n=-1}^{\infty} f_n u_{y,n}, \quad \psi = \sum_{n=-1}^{\infty} f_n \psi_n, \qquad (2.5)$$

where $f_{n+1} \ll f_n$, and $u_{x,n}$, $u_{y,n}$ and ψ_n are $O(1)$. The transverse and longitudinal components of the SW in (2.3) determine the leading magnitudes $f_{-1} = 1/\eta$ and $f_0 = 1$ in the expansion of the velocity field.

2.3. *Examination of $O(1/\eta)$ and $O(1)$ terms*

Equating the $O(1/\eta)$ and $O(1)$ terms, we find the corresponding components of the streamfunction equation and the velocity at the solid boundary are

$$\tfrac{1}{2}\partial_y^4 \psi_{-1} = \partial_t(\partial_y^2 \psi_{-1}), \quad (u_{x,-1}, u_{y,-1})_{y=0} = (0, \exp(\mathrm{i}(t - x + \varphi) - \alpha x)), \qquad (2.6)$$

$$\tfrac{1}{2}\partial_y^4 \psi_0 = \partial_t(\partial_y^2 \psi_0), \quad (u_{x,0}, u_{y,0})_{y=0} = (\chi \mathrm{e}^{\mathrm{i}(t-x)-\alpha x}, 0). \qquad (2.7)$$

The requirements that u_x is bounded far from the solid boundary and that the flow field must satisfy (2.6) and (2.7), and the resultant distribution of the flow field along the solid are all then represented to $O(1/\eta)$ and $O(1)$, respectively, by the equations

$$\left. \begin{aligned} \psi_{-1}|_{y=0} = -\frac{\exp(\mathrm{i}(t - x + \varphi) - \alpha x)}{\mathrm{i} + \alpha}, \quad \partial_y \psi_{-1}|_{y=0} = 0, \\ -\partial_x \psi_{-1}|_{y=0} = \exp(\mathrm{i}(t - x + \varphi) - \alpha x), \end{aligned} \right\} \qquad (2.8)$$

$$\psi_0|_{y=0} = 0, \quad \partial_y \psi_0|_{y=0} = \chi \mathrm{e}^{\mathrm{i}(t-x)-\alpha x}, \quad \partial_x \psi_0|_{y=0} = 0, \qquad (2.9)$$

and by the condition that as $y \to \infty$, ψ_{-1} and ψ_0 are not more singular than y. The leading-order transverse unidirectional flow field is then

$$\psi_{-1} = -\frac{1}{i+\alpha} \exp(i(t - x + \varphi) - \alpha x). \tag{2.10}$$

Its sole component $u_{y,-1}$ simply imitates the transverse component of the solid boundary velocity in (2.8) in order to conserve mass. Equations (2.7) and (2.9) are satisfied by the leading-order Schlichting boundary layer flow field due to a travelling SW

$$\psi_0 = \chi \left(\frac{1}{2} - \frac{i}{2} \right) (1 - e^{-(1+i)y}) \exp(i(t - x) - \alpha x). \tag{2.11}$$

Both flow fields in (2.10) and (2.11) are finite far from the solid boundary. It is interesting to note that (2.11) satisfies only the $O(1)$ longitudinal velocity of the solid surface and remains independent of the $O(1/\eta)$ transverse motion. The leading periodic flow field may thus be represented as a superposition of the unidirectional transverse flow in (2.10) and a solution similar to the classical leading-order Schlichting boundary layer flow in (2.11) but incorporating the behaviour of the fluid as a consequence of travelling waves in addition to the classical treatment of standing waves alone; this result is true regardless of the magnitudes of both flow fields.

We utilize this unusual scaling method in (2.2), where the leading-order term in the asymptotic analysis in (2.5) is large (i.e. $O(1/\eta) \gg 1$), in order to facilitate a direct comparison between magnitudes of the asymptotic flow components in this and earlier studies: (2.11), consistently $O(1)$, represents the leading-order flow both in earlier studies and the second-order flow in the present study.

2.4. *Examination of the $O(\varepsilon/\eta)$ term*

The next correction to the flow satisfies $f_1 = \varepsilon/\eta$ and the streamfunction equation and boundary conditions

$$\tfrac{1}{2} \partial_y^4 \psi_1 = \partial_t (\partial_y^2 \psi_1) - \partial_x \psi_{-1} \partial_y^3 \psi_0, \quad (u_{x,1}, u_{y,1})_{y=0} = (0, 0). \tag{2.12}$$

The requirement that u_x is bounded far from the solid and the other constraints in (2.12) may then be represented to $O(\varepsilon/\eta)$ by

$$\psi_1|_{y=0} = \partial_y \psi_1|_{y=0} = \partial_x \psi_1|_{y=0} = 0 \tag{2.13}$$

and by the condition that, as $y \to \infty$, ψ_1 is not more singular than y. Since we are only interested in the steady drift velocity u_d, we follow Schlichting (1932), Stuart (1966) and Riley (1998, 2001), and decouple the velocity field into its transient and steady components. The steady components of (2.12) and (2.13),

$$\tfrac{1}{2} \partial_y^4 \langle \psi_1 \rangle = -\langle \partial_x \overline{\psi}_{-1} \partial_y^3 \overline{\psi}_0 \rangle, \quad \langle \psi_1 \rangle|_{y=0} = \partial_y \langle \psi_1 \rangle|_{y=0} = \partial_x \langle \psi_1 \rangle|_{y=0} = 0, \tag{2.14}$$

are satisfied by

$$\langle \psi_1 \rangle = \frac{\chi}{2} e^{-2\alpha x} [-e^{-y} \sin(y + \varphi) + y \cos \varphi + (1 - y) \sin \varphi]. \tag{2.15}$$

Note $\overline{\zeta}$ and $\langle \zeta \rangle$ above refer to the real component of the arbitrary function ζ and its time average, such that $\langle \zeta \rangle \equiv (1/2\pi) \int_0^{2\pi} \zeta \, dt$.

Inertial interaction between the two leading-order periodic flow fields results in an $O(\varepsilon/\eta)$ correction to the flow that has a measurable non-vanishing steady component.

In earlier studies, where the flow field is derived for the excitation of one-dimensional acoustic wave, the steady flow component (1.1) is $O(U/c_l)$.

From the ansatz in (2.5), the streamfunction then reads

$$\psi = -\frac{1}{\eta(i+\alpha)} \exp(i(t - x + \varphi) - \alpha x)$$

$$+ \chi \left(\frac{1}{2} - \frac{i}{2}\right) [1 - e^{-(1+i)y}]e^{-\alpha x}e^{i(t-x)} + \cdots; \qquad (2.16)$$

and its steady component is

$$\langle\psi\rangle = \frac{\varepsilon}{\eta}\frac{\chi}{2}e^{-2\alpha x}[-e^{-y}\sin(y+\varphi) + y\cos\varphi + (1-y)\sin\varphi] + \cdots. \qquad (2.17)$$

In the asymptotic limit $y \to \infty$, the dimensional longitudinal and transverse drift velocities found from (2.17) at the outer edge of the boundary layer are then

$$u_{dx} \sim \frac{\varepsilon}{\eta}\frac{\chi U}{2}e^{-2\alpha x}(\cos\varphi - \sin\varphi), \quad \frac{\varepsilon}{\eta}\frac{\chi U}{2} \equiv \frac{\chi U^2}{2}\sqrt{\frac{\rho}{2\mu\omega}}, \qquad (2.18)$$

$$u_{dy} \sim \varepsilon\chi U\beta y\alpha x e^{-2\alpha x}(\cos\varphi - \sin\varphi). \qquad (2.19)$$

The direction and magnitude of the drift velocity (2.18) depend on the phase difference between the longitudinal and transverse components of the SW; its magnitude monotonically decreases as the SW attenuates and does not vanish when the amplitude of the SW excitation is independent of the spatial coordinate, unlike in (1.1). Under pure retrograde motion (e.g. for Rayleigh SAWs, $\varphi = 3\pi/2$), the drift velocity is in the direction of SW propagation whereas under pure prograde motion (e.g. for Sezawa SAWs, $\varphi = \pi/2$), the drift velocity opposes the direction of SW propagation. A similar relation between the drift velocity and phase was obtained by Ramos, Cuevas & Huelsz (2001) under the excitation of a longitudinal oscillating plate that is being impinged by transverse bulk waves; both oscillate at the same frequency.

2.5. *Analysis of closed-channel flow must include bulk acoustic waves in the fluid*

Further analysis is, however, required for microfluidic flows where fluids tend to be in closed structures, such as channels, rather than a half-space as treated before, due to the presence of acoustic waves in both the fluid bulk and the boundary layer. While structural dimensions large compared with the characteristic length of the boundary layer β^{-1} will satisfy the half-space geometry of the theory presented herein to a good approximation, closed geometries under the excitation of SWs have been experimentally and analytically found to support acoustic wave propagation and interaction in the bulk of the fluid, forming standing bulk acoustic waves over long distances (Craster 1996; Hamilton 2003; Tan *et al.* 2009). Bulk acoustic waves are generated from attenuating boundary SWs at the Rayleigh angle and their reflection occurs due to a change in acoustic impedance at the boundary. The amplitude of the reflected wave depends upon the material and configuration details but is very often significant and difficult to suppress in microfluidic platforms. Boundary conditions permitting both a propagating boundary SW and a standing bulk wave tangent to that boundary may be written in generalized dimensional form as (2.1) and

$$(u_x, u_y)_{\beta y \to \infty} = (2\chi U e^{i\omega t}\cos(\delta k x), 0), \qquad (2.20)$$

where $\delta \equiv c/c_l$. The bulk wave is constructed from identical advancing and receding longitudinal waves, emerging from SW-induced vibrations of the channel along the solid boundary (2.20) and describing a bulk wave possessing the frequency, phase and velocity amplitude of the longitudinal component of the SW.

Following a similar procedure, (2.2), (2.3), (2.4) and (2.5) suggest that the $O(1/\eta)$ leading-order component of the streamfunction equation and boundary conditions are given by (2.6), (2.8), and the condition that the streamfunction is not more singular than y as $y \to \infty$; these are satisfied by (2.10). Furthermore, the $O(1)$ component of the streamfunction equation and boundary conditions are given now by (2.7), (2.9), and (2.20). We then decompose the linear $O(1)$ problem to two simplified problems: the flow under the influence of the bulk wave (2.20) and the flow under the influence of the SW in (2.9). The former is described by (2.7), (2.20), and $(u_x, u_y)|_{y=0} = (0, 0)$; a solution is provided by Stuart (1966) and Riley (1998, 2001). The latter, on the other hand, is described by (2.7), (2.9) and a stream function that is no more singular than y as $y \to \infty$, with a solution given by (2.11). The $O(1)$ flow field in the presence of both the SW and the bulk wave is then the superposition of both solutions, given in a dimensionless form as

$$\psi_0 = 2\chi \cos(\delta x) \left\{ y - \frac{1}{2}(1 - \mathrm{i})[1 - \mathrm{e}^{-(1+\mathrm{i})y}]\mathrm{e}^{\mathrm{i}t} \right.$$
$$\left. + \chi \left(\frac{1}{2} - \frac{\mathrm{i}}{2} \right) [1 - \mathrm{e}^{-(1+\mathrm{i})y}]\mathrm{e}^{-\alpha x}\mathrm{e}^{\mathrm{i}(t-x)} \right\}. \tag{2.21}$$

The $O(\varepsilon/\eta)$ steady components of the streamfunction equation and boundary conditions (2.14) together with the requirement that u_x is bounded far from the solid are then satisfied by

$$\langle \psi_1 \rangle = \frac{\chi [\mathrm{e}^{-(y+2\alpha x)}]}{2} \{\mathrm{e}^y[y \cos \varphi + (1 - y) \sin \varphi] - \sin(y + \varphi)$$
$$- 2\mathrm{e}^{\alpha x} \cos(\delta x)\{\mathrm{e}^y[y \cos(x - \varphi) + (y - 1) \sin(x - \varphi)] + \sin(x - y - \varphi)\}\}. \tag{2.22}$$

In the asymptotic limit $y \to \infty$, the dimensional drift velocities along and transverse to the solid boundary,

$$\begin{rcases} u_{dx} \sim \dfrac{\varepsilon}{\eta} \dfrac{\chi U}{2} \mathrm{e}^{-2\alpha kx} \{\{\cos \varphi - \sin \varphi - 2\mathrm{e}^{\alpha kx} \cos(\delta kx) \\ \qquad\qquad \times [\cos(kx - \varphi) + \sin(kx - \varphi)]\}\}, \\ \qquad\qquad\qquad \dfrac{\varepsilon}{\eta} \dfrac{\chi U}{2} \equiv \dfrac{\chi U^2}{2} \sqrt{\dfrac{\rho}{2\mu\omega}}, \end{rcases} \tag{2.23}$$

and

$$u_{dy} \sim \varepsilon \chi \beta U y \mathrm{e}^{-2\alpha kx}\{-\mathrm{e}^{\alpha kx}\{\cos(kx - \varphi)[(-1 + \alpha) \cos(\delta kx) + \delta \sin(\delta kx)]$$
$$+ \sin(kx - \varphi)[(1 + \alpha) \cos(\delta kx) + \delta \sin(\delta kx)]\} + \alpha(\cos \varphi - \sin \varphi)\}, \tag{2.24}$$

conserve both the SW and bulk wavelength scales $\lambda = 2\pi/k$ and $\lambda_l = 2\pi/\delta k$, respectively; this is apparent as we graphically present (2.23) in the next section.

Following Stuart (1966) we may treat the longitudinal drift velocity u_{dx} as the leading-order outer expansion of the inner boundary layer. Ignoring smaller order corrections, matching u_{dx} to the inner expansion of the outer flow field (i.e. the flow outside the boundary layer) is equivalent to using u_{dx} as a slip velocity boundary condition for the outer velocity field: Rayleigh's law of streaming. The longitudinal

drift velocity u_{dx} in (2.18) or (2.23) is then the appropriate asymptotic boundary condition for bulk flow under the influence of a propagating SWs. The $O(\varepsilon)$ transverse drift velocity u_{dy} in (2.19) or (2.24), on the other hand, can usually be ignored. We now seek to validate this theory with a simple experiment.

3. Experiment

A Rayleigh SW is made to propagate along a piezoelectric substrate, inducing boundary layer flow within a microchannel placed atop the substrate as depicted in figure 1(*b*). The Schlichting boundary layer cannot be directly observed since its thickness is generally less than 1 μm under high-frequency excitation, and so we seek to observe the influence of the steady drift velocity on the outer flow field in the vicinity of the solid boundary. The outer flow field is also influenced by Eckart streaming, generated in the bulk of the channel due to the attenuation of acoustic waves emitted, in this case, by the Rayleigh SW (Lighthill 1978). We identify the existence of this particular flow by the steady vortices it generates in the bulk of the channel. This vortical flow has a dispersive influence on the drift velocity developed at the outer edge of the boundary layer. Choosing slender channels (i.e. microchannels) made from material that absorbs and damps the acoustic wave, the Eckart streaming is retarded by viscous effects and reduced in amplitude in its interactions with the channel wall, and in this way we enhance the relative influence of the drift velocity. Nevertheless, weak Eckart streaming was still observed to partially disperse the flow field in the vicinity of the solid substrate over a substantial portion of the channel.

3.1. *Experimental setup*

We employ a 3.2×10^7 Hz Rayleigh SW device comprising a 10 nm chrome/250 nm aluminum interdigital transducer (IDT) electrode patterned using standard UV photolithography on a 0.5 mm thick 128° *Y*-cut, *X*-propagating single-crystal lithium niobate (LN) piezoelectric substrate (Tan, Friend & Yeo 2007*b*; Qi *et al.* 2008). Absorbent material (*α*-gel, Geltec Ltd, Yokohama, Japan), placed at the ends of the substrate, eliminates wave reflections as depicted in figure 1(*b*). The SW is generated by applying a sinusoidal electric voltage to the IDT using a signal generator (SML01; Rhode and Schwarz, North Ryde, NSW, Australia) and amplifier (10W1000C; Amplifier Research, Souderton, PA); an oscilloscope (Wavejet 332/334; LeCroy, Chestnut Ridge, NY) was used to measure the actual voltage across the device. Spatial variations of the velocity amplitude U of the transverse SW along the solid boundary was measured using a laser Doppler vibrometer (LDV; UHF–120, Polytec GmBH, Waldbronn, Germany); the measurements verified that the SW generated here is indeed a propagating Rayleigh SW.

Microchannels, 80 μm thick and 1 mm wide, were prepared by mold-curing 3 mm thick polydimethylsiloxane (PDMS) (Sylgard 184; Dow Corning, Midland, MI) in a standard process (Friend & Yeo 2009) and then filled with a highly dilute suspension (0.003 vol%) of 1 and 5 μm fluorescent polystyrene spheres (Duke Scientific Corp., Fremont, CA) in deionized water (Millipore, Billerica, MA) and attached to the LN substrate following the procedure in Girardo *et al.* (2008). The size of the polystyrene spheres was chosen to ensure the hydrodynamic drag exerted by the fluid dominated the direct acoustic radiation force from the bulk wave in the fluid (Rogers, Friend & Yeo 2010). The flow field in the vicinity of the substrate was acquired using an upright fluorescence microscope coupled to a high-speed camera (BX–FM stereomicroscope and iSpeed camera, Olympus, Yokohama, Japan) and measured both before and after
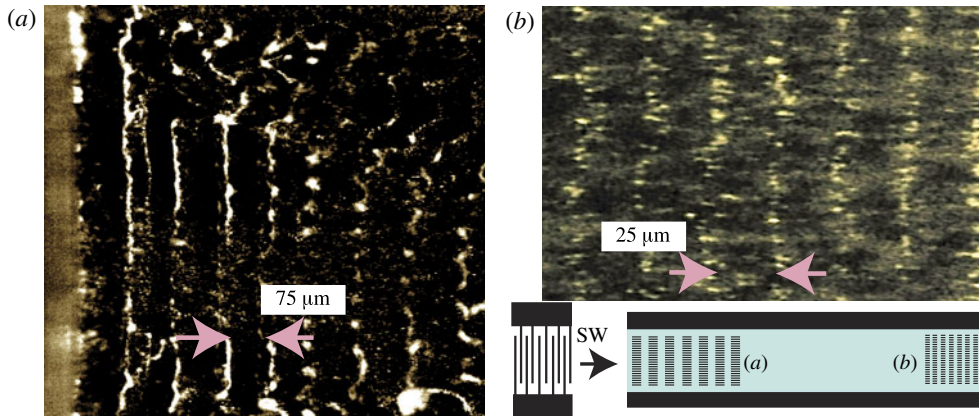
FIGURE 3. (Colour online) (*a*) A top-view illustration of 1 μm particle linear aggregates at (*a*) the front and (*b*) the back edges of the channel, close to and far from the IDT, respectively. As illustrated in the inset that portrays the IDT, channel and particle alignments in (*a*) and (*b*), the SW propagates from left to right with a velocity amplitude $U = 145$ mm s^{-1}. Eckart streaming is observed to disperse the particle alignment in parts of (*a*) and the physical channel's front edge is at the left.

applying voltage to the SW device to confirm the absence of capillary or evaporation effects. The speed of sound, viscosity and density of water were taken to be $c_l = 1500$ m s^{-1}, $\mu_l = 0.89$ mPa s and $\rho_l = 1000$ kg m^{-3}, respectively, and the speed of sound and density in LN were assumed to be $c = 4000$ m s^{-1} and $\rho = 4650$ kg m^{-3}, respectively. These characteristic values may deviate by less than 10 % under normal ambient conditions. The phase difference between the transverse and the longitudinal components is $\varphi = 3\pi/2$ and χ is $O(1)$; both were evaluated under the assumption of an ideal Rayleigh SW (Rudenko & Soluyan 1977).

3.2. *Results and discussion*

Particle alignment in both simple and complex configurations are known to appear under the influence of stationary-wave-induced Schlichting boundary layer flow (Dorrestijn *et al.* 2007; Tan, Friend & Yeo 2007*a*). Here, colloidal patterns in the channel near the substrate boundary were imaged at Rayleigh SW velocity amplitudes of $U = 66, 72, 95, 108, 124, 145$ and 213 mm s^{-1} (deviations from these values are smaller than 1 %) and, regardless of velocity amplitude and particle size, we observe the generation of two distinct patterns in the vicinity of the LN substrate as illustrated in the inset in figure 3. To avoid repetition we will only show patterns arising with 1 μm particles, under $U = 145$ mm s^{-1} velocity amplitude. The particle alignment near the front channel edge, nearer the IDT as indicated with an (*a*) in figure 3(*a*), persists over roughly 4 mm along the channel; a majority of these lines are separated by 70–75 μm, although a discrete Fourier transform of the image also suggests the presence of lines spaced 20–30 μm apart. The first separation length corresponds to one half the SW wavelength $\lambda = 2\pi c/\omega \sim 144$ μm and the second separation length corresponds to one half the bulk wave wavelength at the SW frequency such that $\lambda_l = 2\pi c_l/\omega \sim 47$ μm (deviations from these wavelengths should amount to less than 10 %); since the bulk wave spans the entire length of the channel, it is also likely to affect the particle alignment nearest the IDT.

Further along the channel, beyond 4 mm, the patterns disappear leaving apparently randomly dispersed particles, likely due to both the dispersive influence of Eckart streaming that is most significant in the middle of the channel and the rapid exponential attenuation of the SW in the substrate. The SW attenuation length $\alpha^{-1} \sim F\rho c\lambda/(\rho_l c_l) \sim 1$ mm renders the SW amplitude small beyond $3\alpha^{-1}$–$4\alpha^{-1}$ mm; $F^{-1} \approx 1.4$ is a correction for the anisotropy of the LN substrate (Arzt, Salzmann & Dransfeld 1967; Cheeke & Morisseau 1982).

Roughly 1 mm from the back channel edge, opposite the IDT, the particles once again align in the vicinity of the LN substrate into fine lines with a separation length of approximately 25 μm (figure 3b), corresponding to the bulk wave wavelength at the SW frequency λ_l. Since the SW attenuates before reaching the far end of the channel, we may suppose the excitation there is a SW-induced bulk wave in the fluid domain. The bulk wave is a standing acoustic wave bounded by the fully reflecting air/water interfaces at both channel ends. This hypothesis was assessed by adding water to the channel back end, opposite the IDT, to fill the gap between the channel and the wave absorber, essentially replacing the fully reflecting air/water interface at that end with a poorly reflecting water/wave absorber interface. This was found to suppress the particle alignment in the channel, indicating the bulk wave was likewise absent since pure propagating SW alone generates the drift velocity in (2.18) that does not sustain stagnant areas where particles may aggregate into patterns. We further examine the formation of these aggregation lines by substituting the boundary condition for the SW-induced bulk wave (2.20) into (1.1). This procedure is similar to the classical solution by Stuart (1966) for the drift velocity in a boundary layer excited by a bulk wave. The boundary condition on the substrate in the absence of the Rayleigh SW $(u_x, u_y) = (0, 0)$ at $y = 0$ is then satisfied. The dimensional drift velocity in terms of the bulk wave wavelength $\lambda_l = 2\pi/\delta k$,

$$u_{dx}/U \sim \frac{U}{c_l}\chi^2 \cos(2\pi x/\lambda_l)\sin(2\pi x/\lambda_l), \tag{3.1}$$

is shown in figure 4(b). Each wavelength λ_l contains two stable stagnation points where $u_d = 0$, $\mathrm{d}u_d/\mathrm{d}x < 0$ are satisfied, and where particles align. Two unstable stagnant points, satisfying $u_d = 0$, $\mathrm{d}u_d/\mathrm{d}x > 0$, are also present but represent locations that particles avoid; this is in good agreement with observations.

The difference in particle aggregate patterns near and far away from the IDT, and the different spacing of lines associated with the wavelengths of the bulk wave and SW, respectively, altogether imply a mutual contribution by both the bulk wave and the SW to forming patterns of particles in the channel. We quantify this assertion by substituting the properties of a Rayleigh SW ($\varphi = 3\pi/2$) and a corresponding bulk wave in (2.23) and comparing the expression for the drift velocity

$$u_{dx}/U \sim \frac{\varepsilon}{\eta}\frac{\chi}{2}\{e^{-2\alpha kx} - 2e^{-\alpha kx}\cos(2\pi x/\lambda_l)[\cos(2\pi x/\lambda) - \sin(2\pi x/\lambda)]\}, \tag{3.2}$$

to the patterns in figure 4(a). The good agreement between the stable stagnation regions ($u_d = 0$, $du_d/dx < 0$) generated by the drift velocity (3.2) and the aggregation line patterns in the experiment infers the complicated interaction between SWs and bulk waves within the flow field. The minor difference in the theoretical prediction and experimental result can be attributed to the possible deviations in the characteristic values of the material properties used. Note the denser patterns of particles under $O(\varepsilon/\eta)$ drift flow near the IDT compared with the patterns under $O(\varepsilon)$ drift flow far from the IDT; the density of the patterns is determined in part by a balance between
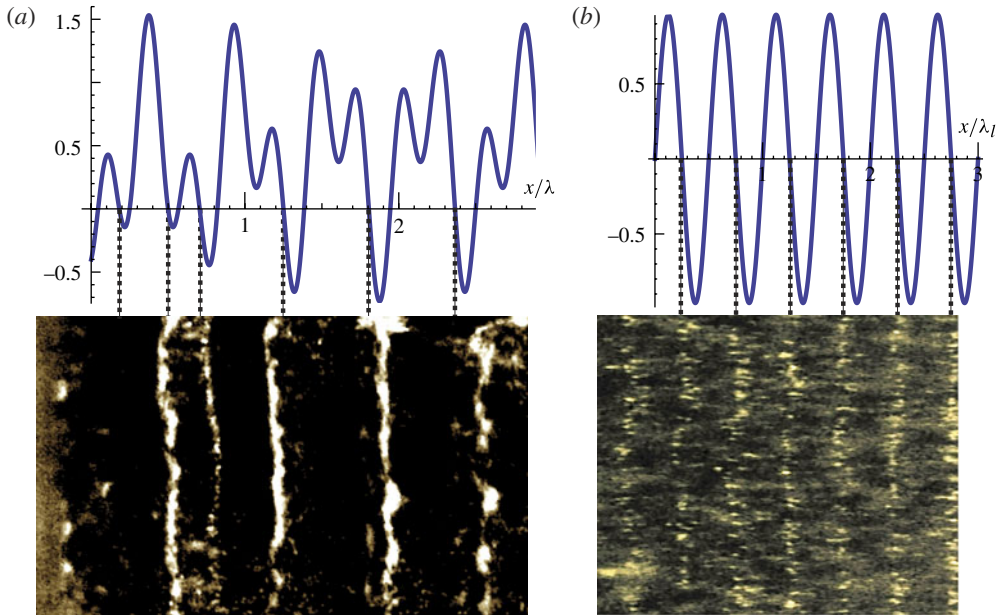
FIGURE 4. (Colour online) Spatial comparison between the theoretical variation of the drift velocity along the solid boundary (positive values refer to flow in the direction of the propagating SW, left to right in the images) and the particle alignments in figure 3 due to the presence of a bulk wave for (*a*) 1 μm polystyrene particles with SW, depicted in (3.2), and (*b*) without SW, depicted in (3.1). Dashed lines connect stable stagnant flow points where particles are predicted to accumulate (driven by the drift flow from both sides) with the particle alignments observed in the experiment: (*a*) $u_{dx}/[(\varepsilon/\eta)_\chi\, U]$; (*b*) $u_{dx}/[(U/c_l)_{\chi^2}\, U]$.

the ordered drift flow and the dispersive effects of particle diffusion and Eckart flow, suggesting that the drift flow is dominant where the particle patterns are most dense and physically illustrating the utility of the scaling used in this study.

4. Conclusions

The classical Schlichting boundary layer theory was extended to include two-dimensional, potentially propagating SW at frequencies and substrate velocities typically employed in microfluidic platforms. The steady drift velocity due to a propagating SW was asymptotically derived, indicating it is $O(\varepsilon/\eta)$ under the excitation of a two-dimensional SW that possesses comparable longitudinal and transverse amplitude components. This result generally dominates the classical $O(U/c_l)$ result that is valid only under the excitation of a simpler one-dimensional acoustic wave.

An additional result was derived for the steady drift velocity in a boundary layer arising from the excitation of both a two-dimensional SW at the solid boundary and an additional standing acoustic wave present throughout the fluid and that possesses similar frequency, phase and velocity characteristics to the SW. This configuration is often present in microfluidic platforms where microflows are enclosed within acoustic wave reflecting structures, such as channels, where SWs give rise to such secondary bulk waves. Weak inertial interaction between the leading superimposed flow fields

resulting from both wave excitations gives rise to a complex, steady and non-vanishing drift velocity that preserves properties from both wave forms.

Good agreement between theory and experiment was found for flow in a microchannel atop a piezoelectric substrate, where high-frequency Rayleigh SW excites a secondary stationary bulk wave in the channel and subsequent Schlichting boundary layer flow; the resultant steady drift velocity observed exhibits characteristics of both wave types in colloidal particle alignments. Finally, the analytical expression derived for the drift velocity may be employed as an effective slip velocity boundary condition for the bulk flow. Further, in the presence of $O(U/c_l)$ slow Eckart streaming, the $O(\varepsilon/\eta)$ drift velocity should dominate the bulk flow. In the presence of $O(1)$ fast Eckart streaming, however, drift velocity effects are likely to be dispersed; nevertheless, the drift velocity exists in the vicinity of the solid substrate and becomes apparent where the bulk flow is stagnant.

REFERENCES

ALVAREZ, M., FRIEND, J. R. & YEO, L. Y. 2008 Surface vibration induced spatial ordering of periodic polymer patterns on a substrate. *Langmuir* **24**, 10629–10632.

ARZT, R. M., SALZMANN, E. & DRANSFELD, K. 1967 Elastic surface waves in quartz at 316 MHz. *Appl. Phys. Lett.* **10**, 165–167.

BRUNET, P., BAUDOIN, M., MATAR, O. & ZOUESHTIAGH, F. 2010 Droplet displacements and oscillations induced by ultrasonic surface acoustic waves: a quantitative study. *Phys. Rev. E* **81**, 036315.

CHEEKE, J. D. N. & MORISSEAU, P. 1982 Attenuation of Rayleigh waves on a LiNbO3 crystal in contact with a liquid He bath. *J. Low Temp. Phys.* **46**, 319–330.

CHLADNI, E. 1787 *Entdeckungen über die Theorie des Klanges*. Weidmanns, Erben und Reich.

CRASTER, R. V. 1996 A canonical problem for fluid–solid interfacial wave coupling. *Proc. R. Soc. Lond.* A **452**, 1695–1711.

DORRESTIJN, M., BIETSCH, A., AÇKALN, T., RAMAN, A., HEGNER, M., MEYER, E. & GERBER, C. H. 2007 Chladni figures revisited based on nanomechanics. *Phys. Rev. Lett.* **98**, 026102.

ECKART, C. 1948 Vortices and streams caused by sound waves. *Phys. Rev.* **73**, 68–76.

FARADAY, M. 1831 On a peculiar class of acoustical figures; and on certain forms assumed by groups of particles upon vibrating elastic surfaces. *Phil. Trans. R. Soc. Lond.* **121**, 299–340.

FRIEND, J. R. & YEO, L. Y. 2009 Fabrication of microfluidics devices using polydimethylsiloxane (PDMS). *Biomicrofluidics* **4**, 026502.

FRIEND, J. R. & YEO, L. Y. 2011 Microscale acoustofluidics: microfluidics driven via acoustics and ultrasonics. *Rev. Mod. Phys.* **83**, 647–704.

GIRARDO, S., CECCHINI, M., BELTRAM, F., CINGOLANI, R. & PISIGNANO, D. 2008 Polydimethylsiloxane–LiNbO3 surface acoustic wave micropump devices for fluid control in microchannels. *Lab on a Chip* **8**, 1557–1563.

HAMILTON, M. 2003 Acoustic streaming generated by standing waves in two-dimensional channels of arbitrary width. *J. Acoust. Soc. Am.* **113**, 153–160.

HODGSON, R. P., TAN, M., YEO, L. Y. & FRIEND, J. R. 2009 Transmitting high power rf acoustic radiation via fluid couplants into superstrates for microfluidics. *Appl. Phys. Lett.* **94**, 024102.

HOLTSMARK, J., JOHNSEN, I., SIKKELAND, T. & SKAVL, S. 1954 Boundary layer flow near a cylindrical obstacle in an oscillating, incompressible fluid. *J. Acoust. Soc. Am.* **26**, 26–39.

HUTCHISSON, E. & MORGAN, F. B. 1931 An experimental study of Kundt's tube dust figures. *Phys. Rev.* **37**, 1155–1163.

LI, H., FRIEND, J. R. & YEO, L. Y. 2008 Microfluidic colloidal island formation and erasure induced by surface acoustic wave radiation. *Phys. Rev. Lett.* **101**, 084502.

LIGHTHILL, J. 1978 Acoustic streaming. *J. Sound Vib.* **61**, 391–418.

LONGUET-HIGGINS, M. S. 1953 Mass transport in water waves. *Phil. Trans. R. Soc. Lond.* **245**, 535–581.

LUONG, T.-D., PHAN, V.-N. & NGUYEN, N.-T. 2011 High-throughput micromixers based on acoustic streaming induced by surface acoustic wave. *Microfluid Nanofluid* **10**, 619–625.

NAM, J., LIM, H., KIM, D. & SHIN, S. 2011 Separation of platelets from whole blood using standing surface acoustic waves in a microchannel. *Lab on a Chip* **11**, 3361.

NYBORG, W. L. 1952 Acoustic streaming due to attenuated plane waves. *J. Acoust. Soc. Am.* **25**, 1–8.

QI, A., YEO, L. Y. & FRIEND, J. R. 2008 Interfacial destabilization and atomization driven by surface acoustic waves. *Phys. Fluids* **20**, 074103.

RAMOS, E., CUEVAS, S. & HUELSZ, G. 2001 Interaction of Stokes boundary layer flow with sound wave. *Phys. Fluids* **13**, 3709–3713.

RAYLEIGH, LORD 1884 On the circulation of air observed in Kundt's tubes and on some allied acoustical problems. *Phil. Trans. R. Soc. Lond.* **175**, 1–21.

RILEY, N. 1965 Oscillating viscous flows. *Mathematika* **12**, 161–175.

RILEY, N. 1986 Streaming from a cylinder due to an acoustic source. *J. Fluid Mech.* **180**, 319–326.

RILEY, N. 1998 Acoustic streaming. *Theor. Comput. Fluid Dyn.* **10**, 349–356.

RILEY, N. 2001 Steady streaming. *Annu. Rev. Fluid Mech.* **33**, 43–65.

ROGERS, P. P., FRIEND, J. R. & YEO, L. Y. 2010 Exploitation of surface acoustic waves to drive size-dependent microparticle concentration within a droplet. *Lab on a Chip* **10**, 2979–2985.

ROSENHEAD, L. (Ed.) 1963 *Laminar Boundary Layers*. Oxford Engineering: Clarendon.

RUDENKO, O. V. & SOLUYAN, S. I. 1977 *Theoretical Foundations of Nonlinear Acoustics*. Plenum.

SCHLICHTING, H. 1932 Calculation of even periodic barrier currents. *Physik. Z.* **33**, 327–335.

SECOMB, T. W. 1978 Flow in a channel with pulsating walls. *J. Fluid Mech.* **88**, 273–288.

SHI, J., HUANG, H., STRATTON, Z., HUANG, Y. & HUANG, T. J. 2009 Continuous particle separation in a microfluidic channel via standing surface acoustic waves (SSAW). *Lab on a Chip* **9**, 3354–3359.

STUART, J. T. 1966 Double boundary layers in oscillatory viscous flow. *J. Fluid Mech.* **24**, 673–687.

TAN, M. K., FRIEND, J. R. & YEO, L. Y. 2007a Direct visualization of surface acoustic waves along substrates using smoke particles. *Appl. Phys. Lett.* **91**, 224101.

TAN, M. K., FRIEND, J. R. & YEO, L. Y. 2007b Microparticle collection and concentration via a miniature surface acoustic wave device. *Lab on a Chip* **7**, 618–625.

TAN, M. K., YEO, L. Y. & FRIEND, J. R. 2009 Rapid fluid flow and mixing induced in microchannels using surface acoustic waves. *Eur. Phys. Lett.* **87**, 1–6.

WANG, C. Y. 2005 On high-frequency oscillatory viscous flows. *J. Fluid Mech.* **32**, 55–68.

WESTERVELT, P. J. 2004 The theory of steady rotational flow generated by a sound field. *J. Acoust. Soc. Am.* **25**, 60–67.

WIXFORTH, A., STROBL, C., GAUER, C., TOEGL, A., SCRIBA, J. & VON GUTTENBERG, Z. 2004 Acoustic manipulation of small droplets. *Anal. Bioanal. Chem.* **379**, 982–991.

YEO, L. Y. & FRIEND, J. R. 2009 Ultrafast microfluidics using surface acoustic waves. *Biomicrofluidics* **3**, 012002.

ZENG, Q., CHAN, H. W. L., ZHAO, X. Z. & CHEN, Y. 2010 Enhanced particle focusing in microfluidic channels with standing surface acoustic waves. *Microelectron. Engng* **87**, 1204–1206.